4962 *Chem. Mater.* **2009,** *21,* 4962–4969
DOI:10.1021/cm902280z

CHEMISTRY OF MATERIALS
Article

Physical Properties, Intrinsic Defects, and Phase Stability of Indium Sesquioxide

Aron Walsh,* C. Richard A. Catlow, Alexey A. Sokol, and Scott M. Woodley

University College London, Department of Chemistry, Materials Chemistry, Third Floor, Kathleen Lonsdale Building, Gower Street, London WC1E 6BT, United Kingdom

Received July 24, 2009. Revised Manuscript Received September 3, 2009

We report an accurate and robust interatomic pair potential for the technologically important transparent conducting oxide indium sesquioxide (In_2O_3). The potential is optimized for the thermodynamically stable bixbyite phase, and it is then used to explore the relative stability and physical properties of five sesquioxide polymorphs and their high-pressure phase transitions. The potential is further employed to investigate the formation of intrinsic defects at the limit of infinite dilution through the embedded Mott−Littleton approach. The anion Frenkel pair is determined to be the lowest energy source of ionic disorder with an energy of formation of 3.2 eV per defect, which can be explained by the presence of intrinsic anion vacancy sites in the bixbyite structure. In contrast, both the cation Frenkel pair (6.9 eV) and Schottky defect (4.4 eV) are less thermodynamically stable. The Schottky formation energy is less in the high pressure phases; however, it remains above 4 eV at elevated pressures.

1. Introduction

Indium sesquioxide (In_2O_3) is a prototypal transparent conducting oxide that is currently used in a wide range of optoelectronic applications, including flat-panel displays, light-emitting diodes, and solar cells.[1,2] Over the past decades, the bulk, surface, and nanostructure properties of the material have attracted substantial experimental interest.[2−15] Electronic structure studies, predominately based on density functional theory (DFT),[16,17] have further contributed to our present knowledge of the structural,[18−21] optical,[18,22,23] and doping[24−28] properties of In_2O_3. However, there remain many open questions regarding the nanoscopic materials chemistry of this system, which lie beyond the limits of purely quantum mechanical approaches. Indeed, little is known about the properties of extended defects, including surfaces, dislocations, and grain boundaries, which are present in fabricated In_2O_3 thin films.

Classical atomistic simulations, which replace the many-body wave function with more tractable pairwise analytic functions, offer a means of performing large-scale simulations with high precision, from which valuable information can be extracted in relation to structure, energetics, defect formation, and ionic transport. Such approaches have significantly advanced our understanding of the extended defects, surfaces, and nanochemistry

*Author to whom correspondence should be addressed. E-mail: a.walsh@ucl.ac.uk.

(1) Edwards, P. P.; Porch, A.; Jones, M. O.; Morgan, D. V.; Perks, R. M. *Dalton Trans.* **2004**, 2995.
(2) Hamberg, I.; Granqvist, C. G. *J. Appl. Phys.* **1986**, *60*, R123.
(3) Granqvist, C. G.; Hultaker, A. *Thin Solid Films* **2002**, *411*, 1.
(4) Nomura, K.; Ujihira, Y.; Tanaka, S.; Matsumoto, K. *Hyperfine Interact.* **1988**, *42*, 1207.
(5) Frank, G.; Köstlin, H. *Appl. Phys. A: Mater. Sci. Process.* **1982**, *27*, 197.
(6) Ohhata, Y.; Shinoki, F.; Yoshida, S. *Thin Solid Films* **1979**, *59*, 255.
(7) Marezio, M. *Acta Crystallogr.* **1966**, *20*, 723.
(8) Wang, S. L.; Chen, C. Y.; Hsieh, M. K.; Lee, W. C.; Kung, A. H.; Peng, L. H. *Appl. Phys. Lett.* **2009**, *94*, 113503.
(9) Weiher, R. L.; Ley, R. P. *J. Appl. Phys.* **1966**, *37*, 299.
(10) Hosono, H. *Thin Solid Films* **2007**, *515*, 6000.
(11) Gassenbauer, Y.; Schafranek, R.; Klein, A.; Zafeiratos, S.; Havecker, M.; Knop-Gericke, A.; Schlogl, R. *Phys. Rev. B* **2006**, *73*, 245312.
(12) King, P. D. C.; Veal, T. D.; Payne, D. J.; Bourlange, A.; Egdell, R. G.; McConville, C. F. *Phys. Rev. Lett.* **2008**, *101*, 116808.
(13) Klein, A.; Körber, C.; Wachau, A.; Säuberlich, F.; Gassenbauer, Y.; Schafranek, R.; Harvey, S. P.; Mason, T. O. Thin Solid Films **2009**, in press (DOI: 10.1016/j.tsf.2009.05.057).
(14) De Wit, J. H. W. *J. Solid State Chem.* **1973**, *8*, 142.
(15) De Wit, J. H. W. *J. Solid State Chem.* **1977**, *20*, 143.
(16) Kohn, W.; Sham, L. J. *Phys. Rev.* **1965**, *140*, A1133.
(17) Hohenberg, P.; Kohn, W. *Phys. Rev.* **1964**, *136*, B864.
(18) Fuchs, F.; Bechstedt, F. *Phys. Rev. B* **2008**, *77*, 155107.
(19) Karazhanov, S. Z.; Ravindran, P.; Vajeeston, P.; Ulyashin, A.; Finstad, T. G.; Fjellvag, H. *Phys. Rev. B* **2007**, *76*, 075129.
(20) Yusa, H.; Tsuchiya, T.; Sata, N.; Ohishi, Y. *Phys. Rev. B* **2008**, *77*, 064107.
(21) Yusa, H.; Tsuchiya, T.; Tsuchiya, J.; Sata, N.; Ohishi, Y. *Phys. Rev. B* **2008**, *78*, 092107.
(22) Walsh, A.; Da Silva, J. L. F.; Wei, S.-H.; Korber, C.; Klein, A.; Piper, L. F. J.; DeMasi, A.; Smith, K. E.; Panaccione, G.; Torelli, P.; Payne, D. J.; Bourlange, A.; Egdell, R. G. *Phys. Rev. Lett.* **2008**, *100*, 167402.
(23) Erhart, P.; Klein, A.; Egdell, R. G.; Albe, K. *Phys. Rev. B* **2007**, *75*, 153205.
(24) Agoston, P.; Albe, K. *Phys. Chem. Chem. Phys.* **2009**, *11*, 3226.
(25) Walsh, A.; Da Silva, J. L. F.; Wei, S.-H. *Phys. Rev. B* **2008**, *78*, 075211.
(26) Hamberg, I.; Granqvist, C. G.; Berggren, K. F.; Sernelius, B. E.; Engström, L. *Phys. Rev. B* **1984**, *30*, 3240.
(27) Tanaka, I.; Oba, F.; Tatsumi, K.; Kunisu, M.; Nakano, M.; Adachi, H. *Mater. Trans.* **2002**, *43*, 1426.
(28) Tomita, T.; Yamashita, K.; Hayafuji, Y.; Adachi, H. *Appl. Phys. Lett.* **2005**, *87*, 051911.

 Published on Web 09/24/2009

of polar solids that include metal oxides (e.g., ZnO,[29,30] CeO_2,[31] VO_2,[32] and MnO_2[33]). Further extension towards multiscale quantum mechanics/molecular mechanics (QM/MM) methods can generate accurate electronic structure information from realistic system sizes.[29,34−37]

The main challenge in using interatomic potentials lies in the parametrization of the appropriate functional form to describe accurately the physical properties of interest. In this work, we report a new potential optimized for the cubic bixbyite phase of In_2O_3. This model reproduces all pertinent structural and physical properties of interest, including the static and high-frequency dielectric constants. The robustness of the proposed potential is checked through investigation of the high-pressure phase stability of a range of known and hypothetical In_2O_3 polymorphs. In addition, we report the formation energy and pressure stability of intrinsic point defects in bixbyite In_2O_3 in the dilute limit. These calculations highlight the low formation energy of anion Frenkel pairs, which is due to the presence of intrinsic anion vacancies in the underlying defective fluorite crystal lattice. In the high-pressure phases, the formation of Schottky defects dominates. The potential model that we have developed will be valuable in subsequent investigations of the physicochemical properties of this material.

2. Computational Details

The interatomic potentials adopted are based on the Born model of ionic solids;[38] indium has a low electronegativity, relative to oxygen, and In_2O_3 features a high static dielectric constant, which is typical of polar metal oxides. Ion−ion interactions are represented through both a Coulomb sum, and a two-body Buckingham potential of the form

$$U_{ij}^{\text{Buckingham}} = A \exp\left(-\frac{r_{ij}}{\rho}\right) - \frac{C}{r_{ij}^6} \quad (1)$$

The short-range energy ($U_{ij}^{\text{Buckingham}}$) is determined by the interaction specific parameters A, ρ, and C, where r_{ij} is the distance between atom i and atom j. To describe the energetics and structural properties accurately, anion polarization must be explicitly taken into account, which is achieved using the shell model.[39,40] The massless shell (charge Y) is connected to a core by a spring (with a spring constant of $k = -F/x$), i.e., the ionic polarizibility is given by

$$\alpha = \frac{Y^2}{k} \quad (2)$$

where the sum of the core and shell charges conserves the formal charge state of the anion.

The defect calculations were performed within the embedded-cluster Mott−Littleton method,[41] which describes an isolated defect center in the true impurity limit; this is unlike the supercell approach that has been adopted in most electronic structure calculations, which is subject to the spurious effects of periodic charged-defect interactions.[42] Within the Mott−Littleton approach, the simulation is divided into an inner region centered around the defect, in which interactions are explicitly treated (region I), and an outer region that responds to the defect perturbation via a linear response approach (region II). In our calculations, the radius of region I was chosen as 10 Å (> 500 atoms) with a 25 Å radius for region IIa (> 5000 atoms); the region IIb continuum commences outside of these spheres and extends to infinity. The calculated defect formation energies are converged to within 50 meV, with respect to the chosen radii. One disadvantage of an interatomic potential approach is that the chemical potential of the individual ions is not directly known; the ion self-energy is defined as zero at infinite separation. Therefore, only the formation energy of stoichiometry-preserving defects can be meaningfully compared in a straight forward fashion in this study. All simulations were performed within the GULP package.[43]

3. Results and Discussions

3.1. Revised Potential Model. Parameterization of the Buckingham potential (eq 1) for In_2O_3 has been reported by Warschow et al.,[44] which itself is derived from the earlier work of McCoy et al.[45] and Bush et al.[46] While their potential, which includes oxygen polarization, reproduces the bixbyite cubic lattice constant, the dielectric properties are less well-described, as shown in Table 1. A potential for In−O and O−O interactions has also been reported by Fisher and Islam,[47] which includes both cation and anion polarization; however, the model was optimized for $Ba_2In_2O_5$ and was not intended to be transferable to the binary system. A third potential can be found in the work of Minervini et al.,[48] which was optimized to reproduce a range of metal oxide structures. While this potential does replicate the experimental lattice constant with minimal error, it is again at the sacrifice of describing the dielectric properties, with errors in excess of 25%, which will be

(29) Catlow, C. R. A.; French, S. A.; Sokol, A. A.; Al-Sunaidi, A. A.; Woodley, S. M. *J. Comput. Chem.* **2008**, *29*, 2234.
(30) Al-Sunaidi, A. A.; Sokol, A. A.; Catlow, C. R. A.; Woodley, S. M. *J. Phys. Chem. C* **2008**, *112*, 18860.
(31) Feng, X.; Sayle, D. C.; Wang, Z. L.; Paras, M. S.; Santora, B.; Sutorik, A. C.; Sayle, T. X. T.; Yang, Y.; Ding, Y.; Wang, X.; Her, Y.-S. *Science* **2006**, *312*, 1504.
(32) Woodley, S. M. *Chem. Phys. Lett.* **2008**, *453*, 167.
(33) Sayle, T. X. T.; Catlow, C. R. A.; Maphanga, R. R.; Ngoepe, P. E.; Sayle, D. C. *J. Am. Chem. Soc.* **2005**, *127*, 12828.
(34) Sherwood, P.; de Vries, A. H.; Guest, M. F.; Schreckenbach, G.; Catlow, C. R. A.; French, S. A.; Sokol, A. A.; Bromley, S. T.; Thiel, W.; Turner, A. J.; Billeter, S.; Terstegen, F.; Thiel, S.; Kendrick, J.; Rogers, S. C.; Casci, J.; Watson, M.; King, F.; Karlsen, E.; Sjøvoll, M.; Fahmi, A.; Schäfer, A.; Lennartz, C. *J. Mol. Struct.: THEOCHEM* **2003**, *632*, 1.
(35) Seijo, L.; Barandiarán, Z. *J. Math. Chem.* **1992**, *10*, 41.
(36) Seijo, L.; Barandiarán, Z. *Int. J. Quantum Chem.* **1996**, *60*, 617.
(37) Grimes, R. W.; Catlow, C. R. A.; Stoneham, A. M. *J. Phys.: Condens. Matter* **1989**, 7367.
(38) Born, M.; Huang, K. *Dynamical Theory of Crystal Lattices*; Oxford University Press: Oxford, MA, 1956.
(39) Dick, B. G.; Overhauser, A. W. *Phys. Rev.* **1958**, *112*, 90.
(40) Lewis, G. V.; Catlow, C. R. A. *J. Phys.: Condens. Matter* **1985**, *18*, 1149.
(41) Mott, N. F.; Littleton, M. J. *Trans. Faraday. Soc.* **1938**, *34*, 485.
(42) Freysoldt, C.; Neugebauer, J.; Van de Walle, C. G. *Phys. Rev. Lett.* **2009**, *102*, 016402.
(43) Gale, J. D.; Rohl, A. L. *Mol. Simul.* **2003**, *29*, 291.
(44) Warschkow, O.; Ellis, D. E.; González, G. B.; Mason, T. O. *J. Am. Ceram. Soc.* **2003**, *86*, 1700.
(45) McCoy, M. A.; Grimes, R. W.; Lee, W. E. *Philos. Mag. A* **1997**, *76*, 1187.
(46) Bush, T. S.; Gale, J. D.; Catlow, C. R. A.; Battle, P. D. *J. Mater. Chem.* **1994**, *4*, 831.
(47) Fisher, C. A. J.; Islam, M. S. *Solid State Ionics* **1999**, *118*, 355.
(48) Minervini, L.; Zacate, M. O.; Grimes, R. W. *Solid State Ionics* **1999**, *116*, 339.

Table 1. Calculated and Experimental Values for the Material Properties of Bixbyite In_2O_3

property	Value					
	experiment	present work	Warschow et al.[44]	Fisher and Islam[47]	Minervini et al.[48]	LDA-DFT[18]
cubic lattice constant, a (Å)	10.117[a]	10.121	10.120	9.689	10.118	10.094
bulk modulus, B (GPa)	194.24[b]	193.77	222.79	224.29	210.25	174
static dielectric constant, ε_0^{11}	8.9−9.5[c]	9.052	6.871	7.533	6.433	
high frequency dielectric constant, ε_∞^{11}	4.0[c]	3.903	3.534	2.376	3.382	3.82
elastic constants						
c_{11} (GPa)		297.75	368.11	288.99	326.18	
c_{12} (GPa)		141.78	150.13	191.94	152.30	
c_{44} (GPa)		76.42	111.26	115.73	126.61	

[a] Data taken from ref 7. [b] Data taken from ref 49. [c] Data taken from ref 2.

Table 2. Buckingham Interatomic Pair Potential Parameters for In_2O_3, with Shell Polarization on Oxygen[a]

pair potential parameters	A (eV)	ρ (Å)	C (eV Å^6)	k (eV/Å^2)	Y (e)
In core−O shell	1498.651	0.3405	33.2		
O shell−O shell	22764.000	0.1490	32.0		
O core−O shell				28	−2.84

[a] The core charges for indium and oxygen are +3.00 and 0.84, respectively.

insufficient to provide an accurate description of charged point defects.

To overcome the limitations of the available potentials, which do not satisfactorily model the key material properties, we perform a revised paramaterization using a weighted fit over a wider range of properties available from experiment, including structure, bulk modulus, and dielectric constants; the resulting potential is detailed in Table 2. As can be observed in Table 1, this potential results in good overall agreement with experiment. In particular, both the static and high-frequency dielectric constants are very well-reproduced. Recent high-pressure powder X-ray diffraction (XRD) reported a bulk modulus of 194 GPa,[49] which is substantially larger than the DFT value of 174 GPa[18] within the local density approximation (LDA); however, this value agrees well with the results from our potential model. A concession in our model lies in the reproduction of the phonon frequencies, which have a range of 106.73−544.99 cm^{-1} at the Brillouin zone center. These compare to the frequency range of 130−650 cm^{-1} that is observed in room-temperature Raman spectra[49] and the frequency range of 205−625 cm^{-1} that is observed in infrared (IR) reflectivity spectra;[50] this is a common compromise in potential fitting, where one must choose between achieving close agreement with the elastic, dielectric, or vibrational properties.

3.2. High-Pressure Polymorphs. The previous results and potential models were based on the thermodynamically stable phase of In_2O_3, the cubic bixbyite structure (space group $Ia\bar{3}$).[51] The unit cell of bixbyite can be viewed as a $2 \times 2 \times 2$ fluorite structured supercell with one-quarter of the anion sites vacant, which are ordered in ⟨110⟩ and ⟨111⟩ directions around each In site. While an early investigation indicated the possibility of an alternative $I2_13$ ground state,[52] our potential model demonstrates that this structure spontaneously relaxes to bixbyite, which is in agreement with recent DFT calculations.[18,19] There are many higher density crystal structures for A_2B_3 stoichiometry, which leads to a variety of metastable high-pressure In_2O_3 phases. To assess the transferability of the proposed potential beyond the cubic bixbyite structure, we have explored the relative stability of competing In_2O_3 polymorphs over a range of 0−70 GPa (in steps of 0.05 GPa): (i) corundum (space group $R\bar{3}c$);[53] (ii) α-Gd_2S_3 (space group $Pnam$);[54] (iii) Rh_2O_3(II) (space group $Pbna$).[55] We have additionally considered the β-Ga_2O_3 structure (space group $C2/m$)[56] and the low-temperature La_2O_3 structure (space group $P\bar{3}m1$),[57] which have not been reported for In_2O_3 to our knowledge, but may be viable at elevated pressures. These structures are illustrated in Figure 1, with the calculated enthalpy−pressure data plotted in Figure 2.

At zero pressure, we found that the energetic ordering of the phases is bixbyite < corundum < Rh_2O_3 < Gd_2S_3 < Ga_2O_3 < La_2O_3, with the La_2O_3 phase being 0.7 eV per formula unit higher in energy than bixbyite. All phases are observed to be stable, with no imaginary phonon frequencies. In the range of 0−70 GPa, two structural transitions are predicted for the lowest enthalpy phase in our $T = 0$ K calculations. The first pressure-induced transition with pressure is from bixbyite to the Rh_2O_3-type phase at 20 GPa, which is stable until ∼45 GPa, where a transition to the α-Gd_2S_3 structure is observed. Rh_2O_3 is a known stable polymorph in this pressure window,[20] and it has also been observed to undergo a phase transition to corundum on decreasing pressure at ∼7 GPa,[20] a crossover point that our data also reproduces (at 9 GPa). Remarkably, the high-pressure stability of α-Gd_2S_3 above 40 GPa was only recently reported from a combination of experiment and DFT calculations.[21] The relevant driving forces for these transitions have been discussed in detail elsewhere.[20,21] The calculated structural and physical properties for the

(49) Liu, D.; Lei, W. W.; Zou, B.; Yu, S. D.; Hao, J.; Wang, K.; Liu, B. B.; Cui, Q. L.; Zou, G. T. *J. Appl. Phys.* **2008**, *104*, 083506.
(50) Sobotta, H.; Neumann, H.; Kühn, G.; Riede, V. *Cryst. Res. Technol.* **1990**, *25*, 61.
(51) Prewitt, C. T.; Shannon, R. D.; Rogers, D. B.; Sleight, A. W. *Inorg. Chem.* **1969**, *8*, 1985.
(52) Zachariasen, W. H. *Skr. Nor. Vidensk.—Akad.,* [*Kl.*] *1: Mat.−Naturvidensk. Kl.* **1928**, *1928*, 165.
(53) Bragg, W. H. *J. Chem. Soc.* **1922**, *121*, 2766.
(54) Prewitt, C. T.; Sleight, A. W. *Inorg. Chem.* **1968**, *7*, 1090.
(55) Shannon, R. D.; Prewitt, C. T. *J. Solid State Chem.* **1970**, *2*, 134.
(56) Geller, S. *J. Chem. Phys.* **1960**, *33*, 676.
(57) Koehler, W. C.; Wollan, E. O. *Acta Crystallogr.* **1953**, *6*, 741.

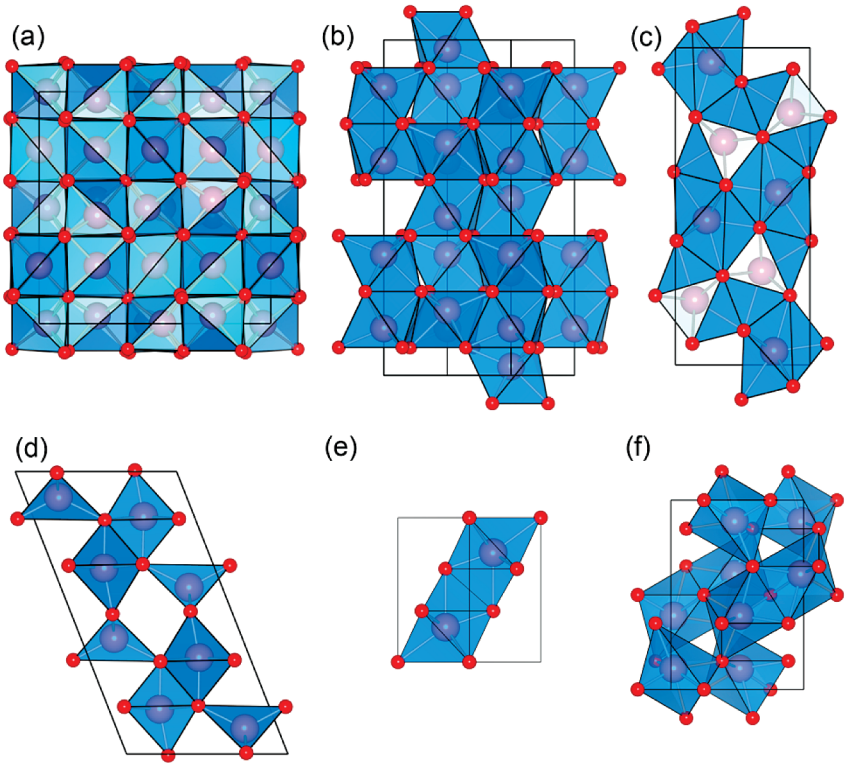

Figure 1. Crystal structure representations of the (a) bixbyite, (b) corundum, (c) α-Gd_2S_3, (d) β-Ga_2O_3, (e) La_2O_3, and (f) Rh_2O_3(II) phases of indium sesquioxide (In_2O_3). The O ions are colored red, with blue polyhedra around the purple In ions.

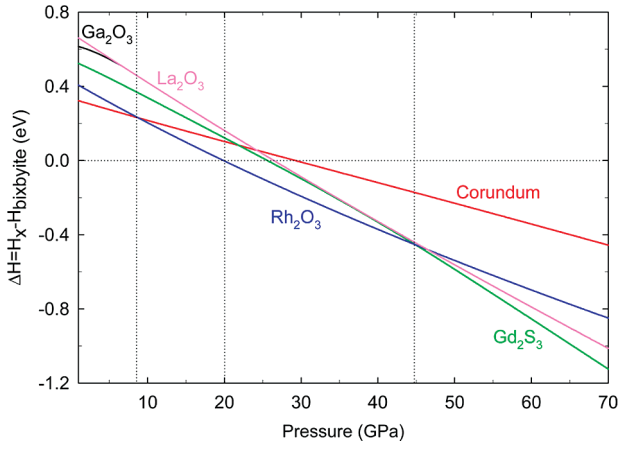

Figure 2. Calculated phase stabilities, per formula unit, of five sesquioxide structures relative to the cubic bixbyite groundstate for In_2O_3 (0 eV). Note that the Ga_2O_3 phase (black line) transitions into the La_2O_3 structure (pink line) above 6 GPa.

bixbyite, Gd_2S_3, Rh_2O_3, and corundum phases at zero pressure and at the two high-pressure transition points are listed in Table 3, from which many trends are apparent: (i) the zero-pressure static dielectric constants are higher in the more-dense phases, and they decrease as the pressure increases; (ii) the high-frequency dielectric constants are smallest in bixbyite, and they increase as the pressure increases; (iii) the Rh_2O_3 structure exhibits the largest bulk moduli at all pressures, whereas the Gd_2S_3 structure exhibits the smallest. Because of the absence of available data, these cannot presently be compared to experimental measurements.

Although the zero-pressure separation between the Ga_2O_3, Gd_2S_3, and La_2O_3 structures is ∼0.2 eV per formula unit, at higher pressures, they come close to being degenerate (within 50 meV per formula unit) at ∼30 GPa before separating again in energy at 45 GPa, which is largely due to a significant compression along the *c*-axis in the β-Ga_2O_3 structure, which produces 7-fold coordinated In sites, similar to the La_2O_3 and Gd_2S_3 phases. Indeed, after 6 GPa, a second-order phase transition from the Ga_2O_3 to La_2O_3 structure is observed. However, at elevated pressures, the Gd_2S_3 structure offers more-efficient packing of the cation polyhedra, resulting in its higher stability above 45 GPa. Thus, because of the small enthalpy differences between 30 GPa and 45 GPa, we expect that the three phases may coexist, along with other related intermediate or possibly amorphous structures.

3.3. Intrinsic Defect Formation. Point-defect formation was investigated for the thermodynamically stable bixbyite phase of In_2O_3. The relevant lattice and interstitial sites involved are illustrated in Figure 3, with their associated Madelung site potentials, which are listed in Table 4. The defect formation energies are listed in Table 5; both structural and electronic (shell) relaxation are determined to be essential in all cases. Removal of an oxygen anion ($V_O^{\bullet\bullet}$) results in a decrease in coordination for four In ions, which contract away from the vacancy site resulting in a reduction in the largest remaining In−O bond length from 2.25 Å to 2.18 Å. Two crystallographically unique In lattice sites are present in bixbyite; both are 6-fold coordinated to oxygen, but the 8b Wyckoff site

Table 3. Calculated Physical Properties of Four In_2O_3 Polymorphs from Three Constant Pressure Simulations at 0, 20, and 45 GPa

	Bixbyite			Rh_2O_3		
property	0 GPa	20 GPa	45 GPa	0 GPa	20 GPa	45 GPa
lattice constants						
a (Å)	10.12	9.83	9.56	7.96	7.71	7.46
b (Å)				5.48	5.35	5.24
c (Å)				5.59	5.45	5.32
volume, V (Å^3 per formula unit)	64.79	59.35	54.64	60.96	56.18	51.95
bulk modulus, B (GPa)	193.77	257.70	327.88	210.59	274.13	344.11
static dielectric constants						
ε_0^{11}	9.05	7.90	7.31	15.33	13.36	12.94
ε_0^{22}	9.05	7.90	7.31	10.66	9.20	8.24
ε_0^{33}	9.05	7.90	7.31	13.80	12.66	13.98
high-frequency dielectric constants						
ε_∞^{11}	3.90	4.13	4.26	4.47	4.65	4.82
ε_∞^{22}	3.90	4.13	4.26	4.34	4.50	4.62
ε_∞^{33}	3.90	4.13	4.26	4.39	4.53	4.66
elastic constants						
c_{11} (GPa)	297.75	334.85	368.99	274.00	334.68	381.10
c_{22} (GPa)	297.75	334.85	368.99	375.11	432.97	492.43
c_{33} (GPa)	297.75	334.85	368.99	343.44	417.65	481.32
c_{44} (GPa)	76.42	83.76	75.00	54.91	58.33	43.35
c_{55} (GPa)	76.42	83.76	75.00	107.13	112.36	110.74
c_{66} (GPa)	76.42	83.76	75.00	107.41	118.21	116.98
c_{12} (GPa)	141.78	219.12	307.33	176.57	234.58	305.63
c_{13} (GPa)	141.78	219.12	307.33	163.96	227.29	310.01
c_{23} (GPa)	141.78	219.12	307.33	115.12	185.28	272.61
	Gd_2S_3			Corundum		
property	0 GPa	20 GPa	45 GPa	0 GPa	20 GPa	45 GPa
lattice constants						
a (Å)	13.21	12.15	11.17	5.49	5.36	5.26
b (Å)	3.35	3.28	3.20			
c (Å)	5.61	5.62	5.65	14.46	13.86	13.22
volume, V (Å^3 per formula unit)	62.01	55.86	50.55	62.82	57.55	52.86
bulk modulus, B (GPa)	114.19	231.29	204.83	198.38	252.54	308.68
static dielectric constants						
ε_0^{11}	13.58	11.01	11.62	9.66	8.14	7.27
ε_0^{22}	14.08	10.44	8.75	9.66	8.14	7.27
ε_0^{33}	10.00	9.22	8.85	15.27	13.63	13.53
high-frequency dielectric constants						
ε_∞^{11}	4.37	4.73	5.18	4.17	4.29	4.40
ε_∞^{22}	4.37	4.65	4.84	4.17	4.29	4.40
ε_∞^{33}	4.24	4.59	4.99	4.33	4.56	4.86
elastic constants						
c_{11} (GPa)	123.23	244.70	237.64	357.16	425.02	495.39
c_{22} (GPa)	329.71	408.12	458.81	357.16	425.02	495.39
c_{33} (GPa)	314.40	367.59	440.39	292.59	314.96	341.05
c_{44} (GPa)	58.66	76.84	76.24	73.31	78.06	57.75
c_{55} (GPa)	99.38	121.44	126.45	73.31	78.06	57.75
c_{66} (GPa)	59.18	93.90	107.61	88.36	97.89	101.93
c_{12} (GPa)	90.19	182.68	210.04	180.45	249.24	336.53
c_{13} (GPa)	144.82	235.86	286.76	116.93	179.88	249.76
c_{23} (GPa)	153.75	224.56	306.45	116.93	179.88	249.76

has high symmetry (S_6) while the 24d site is more distorted (C_2). The removal of an In cation ($V_{In}^{'''}$) results in a relaxation of the neighboring oxygens away from the vacancy center with a substantial contraction of the local In−O bond lengths; e.g., for the 8b indium site, they decrease from 2.11−2.25 Å to 2.04−2.14 Å. The energetic cost for In removal is similar for the 8b and 24b sites; however, it is the 8b site that has a lower energy, by 130 meV, because of its higher site potential.

A natural choice for the anion interstitial is the 16c ($^1/_8,^1/_8,^1/_8$) position−an intrinsic structural anion vacancy (i.e., an occupied anion site in the parent fluorite structure). (See Figure 3.) Other possibilities include the 24d ($^1/_4,0,^1/_4$) and 8a ($^1/_2,^1/_2,0$) sites, which both feature 6-fold oxygen coordination. Occupation of the 16c site by oxygen has been suggested to occur in tin-doped In_2O_3, where the oxygen interstitial compensates the excess Sn charge produced by the aliovalent doping, i.e., the formation of a $[2Sn_{In}^{\bullet}-O_i'']$ charge neutral complex.[5,58] In the intrinsic system, our calculations also predict the 16c interstitial site to be the lowest in energy by more than 1 eV; the oxygen insertion has a minor effect on the local structural environment, as shown in Figure 4.

For the cation interstitial, it could be expected that the 24d or 8a sites would be more stable, because of the shorter initial In−O bond lengths; however, interestingly, the energetic ordering for the unrelaxed defects (8a < 24d < 16c)

(58) Gonzalez, G. B.; Cohen, J. B.; Hwang, J.-H.; Mason, T. O.; Hodges, J. P.; Jorgensen, J. D. *J. Appl. Phys.* **2001**, *89*, 2550.

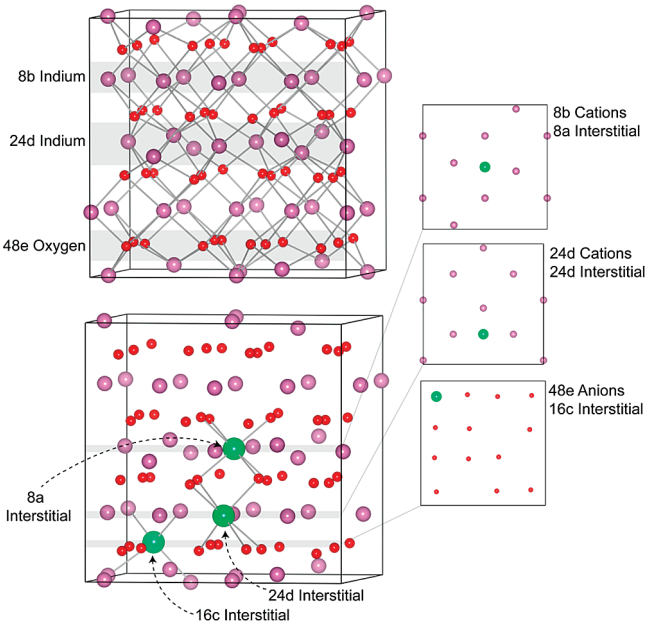

Figure 3. Illustration of high-symmetry ion and interstitial positions within the cubic bixbyite unit cell. The O atoms are colored red (small balls), with purple In and green interstitials (large balls). Two-dimensional ion distributions through (001) planes are shown on the right.

Table 4. Electrostatic Site Potentials for Several High-Symmetry Ion and Interstitial Positions in the Equilibrium Bixbyite Phase of In_2O_3

site	coordination number	potential (V)
In_{In} (8b)	6	−32.33
In_{In} (24d)	6	−32.44
O_O (48e)	4	22.92
V_i (16c)	4	−0.20
V_i (24d)	6	−2.67
V_i (8a)	6	−1.77

Table 5. Calculated Formation and Relaxation Energies for a Range of Intrinsic Defects in Bixbyite In_2O_3: Energetics of Defect Reactions (e.g. Frenkel Pair) are Reported per Defect

defect	unrelaxed (eV)	relaxed (eV)	relaxation energy (eV)
$V_O^{\bullet\bullet}$	35.14	20.99	14.15
V_{In}''' (8b)	78.33	49.92	28.42
V_{In}''' (24d)	78.43	50.05	28.38
O_i'' (16c)	2.09	−14.61	16.70
O_i'' (24d)	5.90	−12.08	17.98
O_i'' (8a)	3.67	−13.29	16.96
$In_i^{\bullet\bullet\bullet}$ (16c)	2.16	−36.21	38.37
$In_i^{\bullet\bullet\bullet}$ (24d)	0.85	−34.89	35.74
$In_i^{\bullet\bullet\bullet}$ (8a)	−0.38	−35.57	35.19
anion Frenkel pair		3.19	
cation Frenkel pair		6.85	
Schottky defect		4.44	
interstitial disorder		4.87	

is overturned by strong relaxation in which the final ordering becomes 16c < 8a < 24d. Both the anion and cation interstitials substantially favor the 16c site. Inspection of the relaxed structures reveals that, upon the addition of indium, there is a concerted outward expansion of the four nearest In ions and an inward contraction of the six O ions, as shown in Figure 4. The resulting In−O separations are in the range of 2.10−2.23 Å, which are close to the ideal bond lengths. In this way, the 16c site offers the space to incorporate the large In cation and can simultaneously satisfy its bonding requirements.

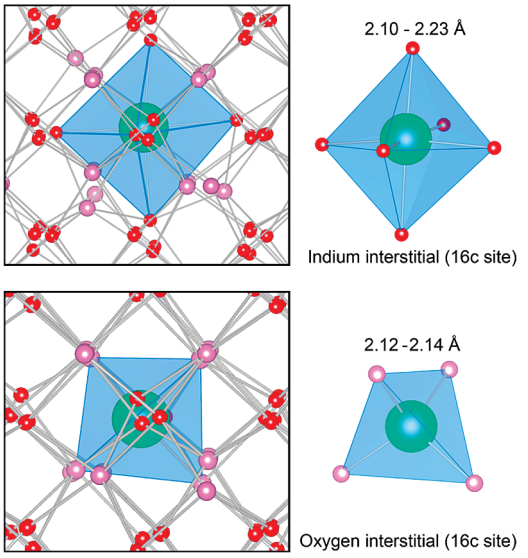

Figure 4. Relaxed geometries around oxygen and indium interstitials (colored green) in bixbyite In_2O_3.

Now, we will consider the energetics of stoichiometric defect formation: the case of intrinsic ionic disorder.[59,60] The Schottky defect represents the removal of In and O ions in stoichiometric units to form vacant lattice sites:

$$2In_{In} + 3O_O \rightleftharpoons 2V_{In}''' + 3V_O^{\bullet\bullet} \quad (3)$$

The associated Schottky defect energy is defined with respect to isolated ion removal and the addition of one formula unit to the bulk lattice ($E[In_2O_3] = -140.60$ eV):

$$E_{Schottky} = \frac{1}{5}(2E[V_{In}'''] + 3E[V_O^{\bullet\bullet}] + E[In_2O_3]) \quad (4)$$

Based on the lowest-energy indium vacancy (the 8b site), the Schottky defect energy is 4.44 eV per defect. Correspondingly, a Frenkel defect is created by the displacement of an occupied lattice site onto an interstitial position, e.g.,

$$In_{In} \rightleftharpoons V_{In}''' + In_i^{\bullet\bullet\bullet} \quad (5)$$

for the cation Frenkel pair, with a formation energy calculated from

$$E_{Frenkel} = \frac{1}{2}(E[V_{In}'''] + E[In_i^{\bullet\bullet\bullet}]) \quad (6)$$

Again, based on the lowest-energy interstitials and vacancies, the anion and cation Frenkel pair energies are 3.19 eV and 6.85 eV per defect, respectively. This energy ordering indicates a stronger preference for the anion Frenkel pair over the other sources of ionic disorder, which is understandable, based on the presence of intrinsic anion vacancy sites in the lattice. In comparison, the cost of creating anion Frenkel pairs in the related TCOs, ZnO and SnO_2 have been reported as 4.40 eV[29]

(59) Smyth, D. M. *The Defect Chemistry of Metal Oxides*; Oxford University Press: Oxford, MA, 2000.
(60) Kröger, F. A. *The Chemistry of Imperfect Crystals*; North−Holland: Amsterdam, 1974.

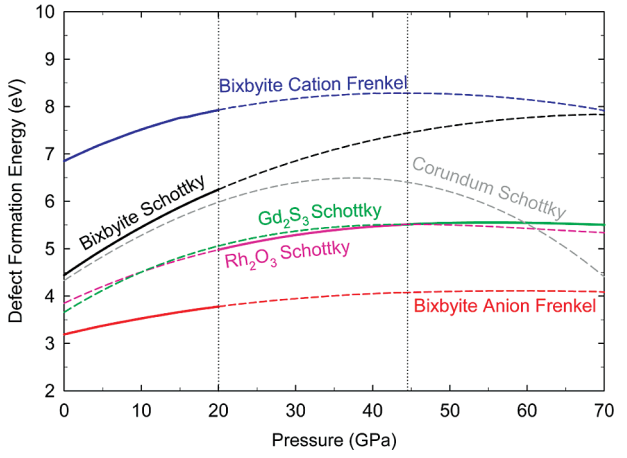

Figure 5. Calculated pressure dependence of the formation energy of three stoichiometric defect pairs in bixbyite In_2O_3. Schottky energies for the three high-pressure phases are shown for comparison, with the stable phase in each pressure region indicated with solid lines.

and 5.53 eV[61] per defect, respectively, using classical simulations, which are substantially higher in energy than In_2O_3, because of the more-efficient packing in the wurtzite and rutile lattices. Because of the low anion Frenkel pair energy, the case of stoichiometric interstitial disorder is also worth considering:

$$E_{\text{Interstitial}} = \frac{1}{5}(2E[\text{In}_i^{\bullet\bullet\bullet}] + 3E[\text{O}_i''] - E[\text{In}_2\text{O}_3]) \qquad (7)$$

which is observed to cost 4.87 eV per defect, which is moderately higher than the Schottky defect energy but still lower than the formation energy of the cation Frenkel pair.

We have further investigated the pressure dependence of the three key stoichiometric defects over the range of 0−70 GPa (Figure 5). Here, isochoric point defect formation is calculated within a lattice that has been optimized at a fixed pressure. In this range, the anion Frenkel pair increases in energy from 3.19 eV to 4.09 eV; while the cost of oxygen vacancy formation decreases as the pressure increases, the cost of the oxygen interstitial increases at a faster rate. The same interplay is observed for the cation Frenkel pair, which increases from 6.85 eV to 7.91 eV. The rate of change for the Schottky defect is much greater, which increases from 4.44 eV to 7.83 eV; a similar pressure dependence for Schottky formation has previously been reported in $MgSiO_3$.[62] However, to provide tangible insight into the high-pressure defect behavior, we must consider the appropriate stable phases. For the high-pressure phases, which are significantly denser than bixbyite, the Schottky defect is the dominant source of ionic disorder. The associated ion vacancy and Schottky energies for the corundum, Rh_2O_3 and Gd_2S_3 phases, are compared in Table 6. At zero pressure, Schottky defect formation is very similar in the bixbyite and corundum phases; although the formation energy is lower in the Rh_2O_3 and Gd_2S_3 phases, it is still significantly costly at > 3.5 eV.

Table 6. Calculated Ion Vacancy and Schottky Defect Formation Energies for the Bixbyite, Corundum, Rh_2O_3, and Gd_2S_3 Phases of In_2O_3 at Zero Pressure

phase	$V_O^{\bullet\bullet}$ (eV/defect)	V_{In}''' (eV/defect)	Schottky defect (eV/defect)
bixbyite	20.99	49.92	4.44
corundum	21.39	48.88	4.33
Rh_2O_3	20.70	48.66	3.85
Gd_2S_3	20.20	48.87	3.66

The pressure dependence of Schottky defect formation for all four phases is compared in Figure 5. At zero pressure, defect formation in the Rh_2O_3 (Gd_2S_3) phase is 0.59 eV (0.79 eV) more favorable than for bixbyite. At 20 GPa, Schottky defect formation in the Rh_2O_3 phase is 4.98 eV, whereas at 45 GPa, it is 5.52 eV in the Gd_2S_3 phase. Therefore, the cost of creating intrinsic ionic disorder is high in all stable phases at elevated pressures, which suggests that ionic disorder will not be appreciable without the influence of extrinsic impurities or dopants. For the corundum phase, the initial Schottky formation energy is similar to bixbyite and shows a similar pressure dependence up to 40 GPa, but then begins to decrease because of a reduction in energy of the oxygen vacancy in the corundum structure at higher pressures.

4. Conclusions

We have reported a revised interatomic potential for In_2O_3, which both reproduces the structural and physical properties of the thermodynamically stable bixbyite phase and marks a significant improvement over the previously reported potentials. Calculation of the relative stability of five high-pressure phases up to 70 GPa revealed transition pressure ranges in good agreement with both experimental observations and ab initio electronic structure calculations. Furthermore, we investigated the formation of intrinsic defects in the bixbyite lattice, including all possible ion vacancies and interstitials. The results revealed a marked preference for the anion Frenkel pair arising from the presence of intrinsic anion vacancy sites in the underlying defective fluorite lattice. However, at high pressures, the Schottky defect energy is reduced when the appropriate stable phases are considered. The formation energies exceed 3 eV for all stoichiometric defects; therefore, intrinsic ionic disorder is not expected to be appreciable in any In_2O_3 polymorph grown under equilibrium conditions.

Empirically, In_2O_3 is known as an *n*-type electron conductor, because of oxygen substoichiometry, and progress in transparent oxide optoelectronics applications relies on the fabrication of *p*-type materials (for *p*−*n* junctions).[10,63−65] We are currently investigating approaches to explore the redox properties using a combination of classical and quantum chemical approaches, which would shed light on the atomistic origins of the

(61) Freeman, C. M.; Catlow, C. R. A. *J. Solid State Chem.* **1990**, *85*, 65.
(62) Watson, G. W.; Wall, A.; Parker, S. C. *J. Phys.: Condens. Matter* **2000**, 8427.
(63) Ogo, Y.; Hiramatsu, H.; Nomura, K.; Yanagi, H.; Kamiya, T.; Hirano, M.; Hosono, H. *Appl. Phys. Lett.* **2008**, *93*, 032113.
(64) Scanlon, D. O.; Morgan, B. J.; Watson, G. W.; Walsh, A. *Phys. Rev. Lett.* **2009**, *103*, 096405.
(65) Godinho, K. G.; Watson, G. W.; Walsh, A.; Green, A. J. H.; Payne, D. J.; Harmer, J.; Egdell, R. G. *J. Mater. Chem.* **2008**, *18*, 2798.

n-type behavior and assess the possibility of *p*-type doping, in addition to highlighting the potential for electrochemical applications.

Acknowledgment. A.W. would like to acknowledge funding from a Marie-Curie Intra-European Fellowship from the European Union under the Seventh Framework Programme. The authors acknowledge the use of the UCL Legion High Performance Computing (HPC) Facility, and associated support services, in the completion of this work. The work has also been supported by an EPSRC Portfolio Partnership (Grant No. ED/D504872).